

ON THE STRAIN ENGINEERING OF GRAPHENE

A Thesis
Presented to
The Academic Faculty

by

Nicolas Kerszberg

In Partial Fulfillment
of the Requirements for the Degree
Master of Science in the
School of Civil and Environmental Engineering

Georgia Institute of Technology
December 2014

COPYRIGHT ©2014 NICOLAS KERSZBERG

ON THE STRAIN ENGINEERING OF GRAPHENE

Approved by:

Professor Phanish Suryanarayana, Advisor
School of Civil and Environmental Engineering
Georgia Institute of Technology

Professor Ting Zhu
School of Mechanical Engineering
Georgia Institute of Technology

Professor Markus Kindermann
School of Physics
Georgia Institute of Technology

Date Approved: December 2014

ACKNOWLEDGEMENTS

I would like to express my deep gratitude to my advisor, Prof. Phanish Suryanarayana, for his guidance, patience and expertise, and the committee members Profs. Ting Zhu and Markus Kindermann, for their time and contributions. I would also like to thank my family for giving me the unwavering support I needed.

TABLE OF CONTENTS

ACKNOWLEDGEMENTS	iii
TABLE OF CONTENTS	iv
LIST OF TABLES	v
LIST OF TABLES	v
LIST OF FIGURES	vi
LIST OF FIGURES	vi
SUMMARY	vii
I BACKGROUND	1
II METHODOLOGY	3
2.1 Unit Cell	3
2.2 Deformation	4
2.3 Reciprocal Space and Brillouin Zone	5
2.4 Bloch's Theorem Exploiting Periodicity	6
2.5 Brillouin Zone Sampling	7
2.6 Generating Input Files and Defining the Strain Space	8
III RESULTS	10
3.1 Convergence	10
3.2 Uniaxial Strain	12
3.3 Biaxial Strain	14
3.4 Shear Strain	15
3.5 Angular Uniaxial Strain	16
3.6 Traversal of In-Plane Strain Space	18
3.7 Asymmetrical Biaxial Strain	19
IV CONCLUSION	22
APPENDIX A — SAMPLE ABINIT INPUT FILE	23
APPENDIX B — BAND STRUCTURE PLOTS	25

Bibliography **27**

LIST OF TABLES

1	Convergence data for acell and ecut in graphene	11
2	States of strain with high band gaps	19

LIST OF FIGURES

1	The Unit Cell	4
2	The Brillouin Zone	6
3	Random Brillouin Zone Sampling	8
4	Strain vs. band gap for uniaxial strain in zigzag direction	13
5	Strain vs. band gap for uniaxial strain in armchair direction	14
6	Strain vs. band gap for biaxial strain	15
7	Strain vs. band gap for shear strain	16
8	Angle vs. band gap for uniaxial strain when $\varepsilon = 0.1$	17
9	Angle vs. band gap for uniaxial strain when $\varepsilon = 0.15$	18
10	Angle vs. band gap for uniaxial strain when $\varepsilon = 0.2$	18
11	Graphical representation of band gap opening as a function of ε_{ac} and ε_{zz} .	20
12	Graphical representation of band gap opening as a function of ε_{ac} and ε_{zz} .	21
13	Band Structure	25
14	Band Structure	26

SUMMARY

Graphene is renowned for its extraordinary mechanical, electronic, optical, and thermal properties. However, the absence of a band-gap limits its usefulness in practical applications. If it were possible to engineer graphene to exhibit a band gap, this would open the doors to a wide range of applications for the material, such as use in sensors, solar cells, and energy storage devices. This thesis attempts to definitively state the possibility of opening a band gap through in-plane strain engineering of graphene. This is inspired by the fact that the electronic properties of a number of materials have already been shown to be influenced by deformations. In this work, electronic structure calculations based on Density Functional Theory (DFT) in conjunction with finite deformation theory are employed to determine the effect of in-plane strains on the band gap of graphene. It can be affirmed that a band gap does not appear in graphene under uniaxial or biaxial strains, while moderate gaps do appear under large shear strains (20%). Notably, significant band gaps have been found to open under asymmetrical biaxial strain, particularly in the range of -15% to -20% (compression) in the armchair direction. The highest gap obtained was approximately 1 eV, identified at 11% strain in the zigzag direction and -20% in the armchair direction.

CHAPTER I

BACKGROUND

The graphene revolution started in 2004 when individual layers were isolated using the scotch tape technique [1, 2]. As a two dimensional hexagonal arrangement of carbon atoms, graphene exhibits fascinating mechanical, electronic, optical, and thermal properties, while remaining lightweight, flexible and strong [3, 4]. Among its notable electronic properties is the high electron and hole mobility, allowing it to conduct electricity exceptionally well, comparable to that of a metal [5]. This high charge mobility would be prized in electronic devices if it could be accompanied by a band gap [4]. Efforts have been made to induce a band gap in the material, such as epitaxial growth [6], bilayer graphene [7], applied electric fields [8] and strain engineering [9, 10, 11, 12, 13, 14]. The various attempts at strain engineering have included periodic inhomogeneous strains [9], uniaxial strain [10, 11, 12, 13], and shear strains [14]. Large gaps can be achieved in carbon nanotubes, which are sheets of graphene rolled into cylinders, as well as one dimensional nanoribbons, but the precision involved with the production of these allotropes is restrictive [2, 15].

Through Density Functional Theory (DFT) [16] calculations, Ni et al. [10] originally showed that a gap of approximately 0.3 eV opened for graphene under 1% uniaxial tensile strain in the zigzag direction. However, after realizing an error in their calculations [17], they concluded that the critical uniaxial strain required to open a band-gap is around 26.5%. Using ab-initio calculations, Gui Gui et al. [11] showed that with a symmetrical strain distribution (biaxial), graphene does not open a band gap. Under strain parallel to C-C bonds (armchair direction) however, the band gap is 0.486 eV at 13.1% strain, and decreases under larger deformation, and for strain perpendicular to C-C bonds (zigzag direction), the band gap is 0.170 eV at 4.91% strain and decreases under larger deformation. Choi et al. [12] determined from ab initio calculations that graphene remained semi-metallic (i.e. no significant band gap) under uniaxial strain of up to 30%. Using the Tight-Binding method,

Cocco et al. [14] found that gaps of up to 0.9 eV can be obtained under strain below the failure point, and that the most effective way to control the gap opening is to combine a shear and an armchair uniaxial deformation. Naumov and Bratkovsky [9] have found using ab-initio methods that by using uniform strains, gaps do not occur, but that it is possible to open a gap by a sine-like inhomogeneous deformation applied along a direction other than armchair, with the largest gap along the zigzag direction. The consensus appears to be that strain engineering of graphene is possible but not practical, as the strains necessary exceed the mechanical limit of the material.

CHAPTER II

METHODOLOGY

As with many of the attempts mentioned in the previous chapter, we perform first principles-based DFT [16] calculations. Specifically, we utilize the software ABINIT [18, 19] for performing the electronic structure calculations. We envisage traversing the in-plane strain space, in order to affirm whether practical strains indeed do not open a gap, or if there are possibilities to do so that have not yet been discovered. We are limited to in-plane strains due to the periodic boundary conditions imposed in the ABINIT software. Any out-of-plane strains would be translated periodically across unit cells and would not have the effect of bending or torsion, but rather of corrugation.

We begin by establishing the geometry of graphene that is necessary to translate into a computational model. The distortion of this geometry is then performed methodically using finite deformation theory. Since it is claimed that only strains exceeding the mechanical limit open gaps, we will limit the definition of feasible strains to those below 20%, since the mechanical limit of graphene is not significantly higher than 25% strain [20, 21] and higher strains are inevitably more difficult to achieve in practice. Finally, the resulting data is analyzed for feasibility, i.e. practical strains, and the opening of a band gap. The notation used throughout will be a bar for vectors, \bar{a} , and bold face, \mathbf{A} , for tensors and matrices.

2.1 Unit Cell

The crystal structure of graphene is arranged in a two dimensional hexagonal pattern [1, 2, 3, 4, 5], which is different from the three dimensional hexagonal close-packed (HCP) lattice. From this structure, one can specify a primitive unit cell, which is a volume (in this case area) constructed around a lattice point that fills all space when translated periodically. The unit cell in Figure 1 was chosen to provide a symmetric working geometry. The resulting parallelogram can be described by the vectors

$$\begin{aligned}\bar{a}_1 &= a_0 \left(\frac{\sqrt{3}}{2}, \frac{3}{2}, 0 \right), \\ \bar{a}_2 &= a_0 \left(-\frac{\sqrt{3}}{2}, \frac{3}{2}, 0 \right), \\ \bar{a}_3 &= c_0(0, 0, 1),\end{aligned}$$

where a_0 is the interatomic distance and c_0 is the distance between layers.

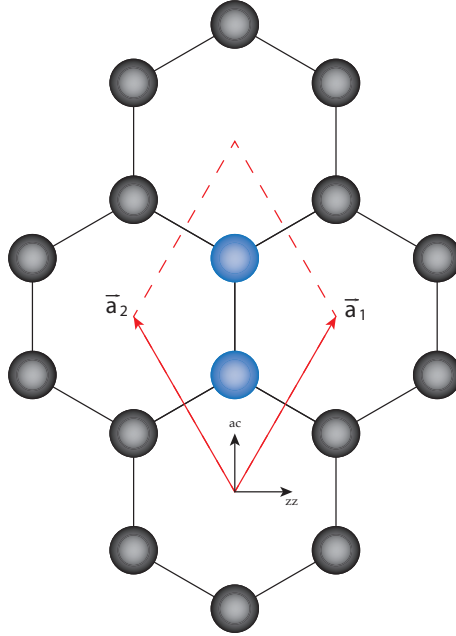


Figure 1: One unit cell within the hexagonal structure, defined by \bar{a}_1 and \bar{a}_2 . The atoms, represented by blue circles, are positioned at $(\frac{1}{3}, \frac{1}{3}, 0)$ and $(\frac{2}{3}, \frac{2}{3}, 0)$ in reduced coordinates with respect to the lattice vectors; that is, $\frac{1}{3}\bar{a}_1 + \frac{1}{3}\bar{a}_2 + 0\bar{a}_3$ is the position of the bottom atom, and $\frac{2}{3}\bar{a}_1 + \frac{2}{3}\bar{a}_2 + 0\bar{a}_3$ is the position of the top atom.

2.2 Deformation

The strains under consideration far exceed the limits of infinitesimal strain theory. Infinitesimal strains are very small and only approximated to the first order by linear elasticity using the Lagrangian strain tensor [22]:

$$\begin{aligned}\mathbf{E} &= \mathbf{F}^T \mathbf{F} - \mathbf{I} \\ &\approx \boldsymbol{\varepsilon}\end{aligned}$$

where ε is the linear infinitesimal strain tensor. We run simulations for strains of up to 25%, and therefore the deformation gradient \mathbf{F} of finite deformation theory must be utilized. The reference configuration is taken to be the one described by the undeformed lattice vectors \bar{a}_1 and \bar{a}_2 . To obtain the deformed configuration, the deformation gradient is determined from the strain tensor \mathbf{E} :

$$\begin{aligned}\mathbf{E} &= \begin{pmatrix} \varepsilon_{11} & \varepsilon_{12} & 0 \\ \varepsilon_{21} & \varepsilon_{22} & 0 \\ 0 & 0 & 0 \end{pmatrix} \\ \mathbf{F}^T \mathbf{F} &= 2\mathbf{E} + \mathbf{I} \\ \mathbf{F} &= \mathbf{V}(\mathbf{D})^{1/2} \mathbf{V}^T\end{aligned}$$

where ε_{11} is the strain in the zigzag direction, ε_{22} is the strain in the armchair direction, $\varepsilon_{12} = \varepsilon_{21}$ is the shear strain, \mathbf{D} is a diagonal matrix containing the eigenvalues (principal strains) of $\mathbf{F}^T \mathbf{F}$, and \mathbf{V} is a matrix whose columns are the eigenvectors (principal directions) corresponding to the eigenvalues in \mathbf{D} .

The deformed lattice vectors \bar{a}'_i can be found by taking the matrix product with the deformation gradient:

$$\mathbf{F} \bar{a}'_i = \bar{a}_i, \quad i = 1, 2, 3.$$

Note that \bar{a}'_3 will always be $(0, 0, 1)$ regardless of deformation.

2.3 Reciprocal Space and Brillouin Zone

Using the relation [23]

$$\bar{a}_i \cdot \bar{b}_j = 2\pi \delta_{ij},$$

the reciprocal space vectors can be determined to be

$$\begin{aligned}\bar{b}_1 &= 2\pi \frac{\bar{a}_2 \times \bar{a}_3}{\bar{a}_1 \cdot \bar{a}_2 \times \bar{a}_3} \\ &= \frac{2\pi}{a_0} \left(\frac{\sqrt{3}}{3}, \frac{1}{3}, 0 \right), \\ \bar{b}_2 &= 2\pi \frac{\bar{a}_3 \times \bar{a}_1}{\bar{a}_1 \cdot \bar{a}_2 \times \bar{a}_3}\end{aligned}$$

$$= \frac{2\pi}{a_0} \left(-\frac{\sqrt{3}}{3}, \frac{1}{3}, 0 \right),$$

$$\bar{b}_3 = \frac{2\pi}{c_0} (0, 0, 1).$$

These vectors can be used to define the Brillouin zone, as can be seen in Figure 2.

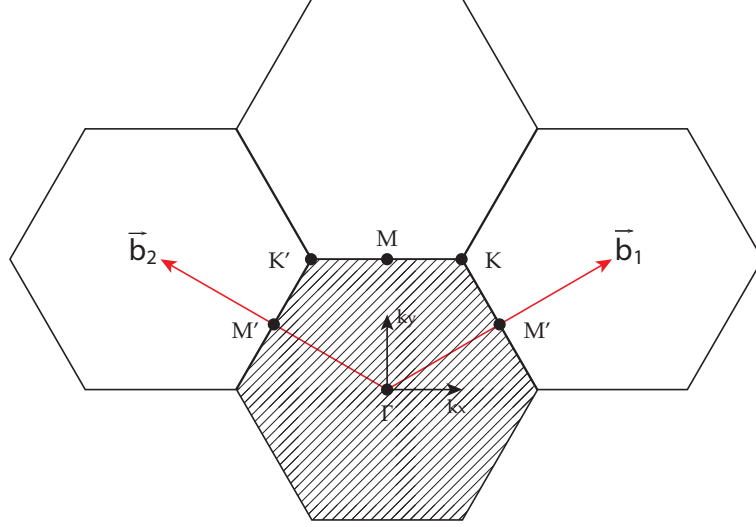


Figure 2: The reciprocal space lattice in the shaded region defined by the vectors \bar{b}_1 and \bar{b}_2 . The high symmetry points are Γ , K , M , K' , and M' . The coordinates are found in a similar fashion as the atom positions. Γ is $0\bar{b}_1 + 0\bar{b}_2 + 0\bar{b}_3$, K is $\frac{1}{3}\bar{b}_1 + \frac{2}{3}\bar{b}_2 + 0\bar{b}_3$, M is $\frac{1}{2}\bar{b}_1 + \frac{1}{2}\bar{b}_2 + 0\bar{b}_3$, K' is $\frac{2}{3}\bar{b}_1 + \frac{1}{3}\bar{b}_2 + 0\bar{b}_3$, and M' is $\frac{1}{2}\bar{b}_1 + \bar{b}_2 + 0\bar{b}_3$ or $0\bar{b}_1 + \frac{1}{2}\bar{b}_2 + 0\bar{b}_3$.

2.4 Bloch's Theorem Exploiting Periodicity

Given that the governing equation in DFT is an eigenvalue problem, Bloch's Theorem [23] can be used to reduce all the calculations to the unit cell.

Using the lattice and reciprocal vectors, as well as the wavefunction $\psi(\vec{r})$, the eigenfunction relation $u(\vec{r}) = e^{-i\vec{k}\vec{r}}\psi(\vec{r})$ where $\vec{k} = \sum_{i=1}^3 \bar{x}_i \bar{b}_i$, and the translation operator $\psi(\vec{r} + \vec{a}_i) = e^{i\vec{x}_i} \psi(\vec{r})$, we can use Bloch's Theorem to establish periodic boundary conditions:

$$\begin{aligned} u(\vec{r} + \vec{a}_i) &= e^{-i\vec{k}\vec{r}} \psi(\vec{r} + \vec{a}_i) \\ &= e^{-i\vec{k}\vec{r}} e^{-i\vec{x}_i} e^{i\vec{x}_i} \psi(\vec{r}) \\ &= e^{-i\vec{k}\vec{r}} \psi(\vec{r}) \end{aligned}$$

$$= u(\bar{r}).$$

In effect, any translation by a vector \bar{a}_i , i.e. a shift equal to the distance of one lattice, will result in the same value for the eigenfunction $\psi(\bar{r})$. In this way we can establish an infinite space which repeats with periodicity \bar{a} .

2.5 Brillouin Zone Sampling

When studying materials, the band structure can be obtained from the high-symmetry points of the Brillouin zone. Under different strains, however, and especially shear, the points will not move in a manner that will be captured by only specifying the high symmetry points, or straight lines between them, and under large deformations we must objectively assume they could be anywhere in the Brillouin zone. The difficulty in finding the true minimum band gap in strained graphene lies in accurately locating the correct k-point in the Brillouin zone. Not locating this would result in detecting erroneously large band gaps.

The method conceived was to randomly sample the Brillouin zone with a large amount of k-points in order to statistically reduce the likelihood of missing the point or area with the lowest gap. After sampling the entire Brillouin zone, the k-point that contained the lowest band gap was identified and more k-points were randomly sampled in a smaller area in the vicinity of this point to further increase accuracy.

An inconvenience of ABINIT is that it fails to print out the k-point number in the output file past 9,999 points. For this reason, coupled with the character size limits in the input file which are rapidly surpassed with large amounts of k-points specified with 14 decimal places, the decision was made to limit one input file to 9,999 k-points. To compensate, several iterations would be run of each input file containing a unique deformation gradient, each adding 9,999 more points to our data. Given the continuous and smooth nature of the band structure, it is expected that nearby points that are not sampled will not have band gaps that are drastically different. The result of this kind of sampling can be seen in Figure 3.

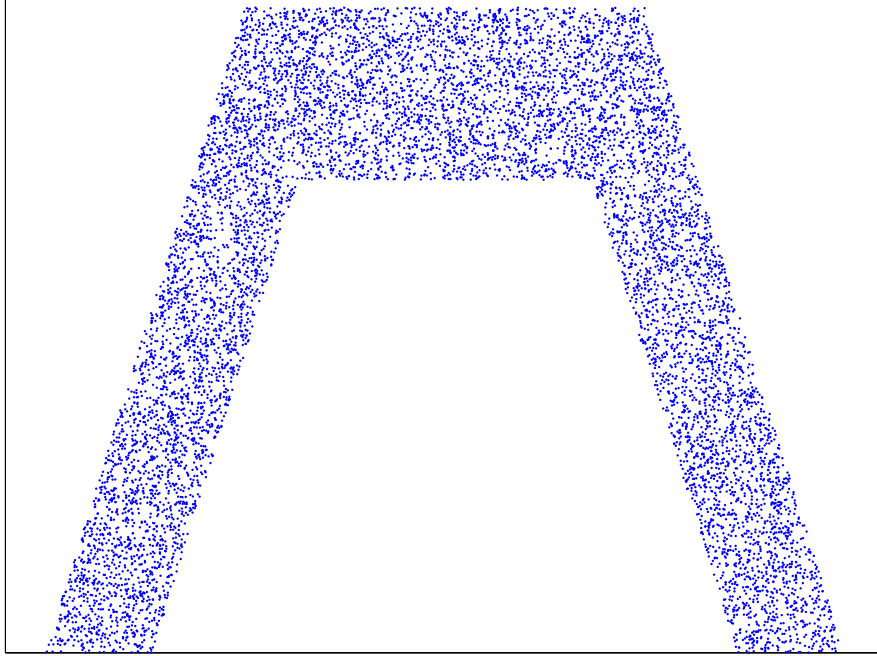


Figure 3: 9,999 k-points randomly generated in the upper half of the Brillouin zone shown in Figure 2.

2.6 Generating Input Files and Defining the Strain Space

ABINIT input files were created by using MATLAB[®] to simultaneously calculate all the values derived from the deformation gradient and write the appropriate ABINIT commands with their corresponding values to file. The decision was made to have a maximum strain of 25%, since this is near the failure point of graphene, and any results past it would not be useful. Each value must also have a corresponding negative value to account for both tension and compression.

To illustrate, uniaxial strain in the zigzag direction was achieved by specifying the zigzag component ε_{11} of the strain matrix and having that variable loop from -0.25 to 0.25 in steps of 0.05. Setting $\varepsilon = 0.25$ is equivalent to saying 25% tensile strain. This results in separate input files for -25%, -20%, -15%, etc. strain in the zigzag direction only. Combinations of the variables for strain in the armchair direction and in shear can subsequently be added.

In order to cover the entire strain space, each possible permutation of these variables must be generated, taking into account that $\varepsilon_{12} = \varepsilon_{21}$. The step value was chosen as 5%, since these loops create 1,331 permutations. Steps of, for example, 1% would generate 132,651 permutations. Considering that each permutation is an input file that needs to run for several hours and the memory that the resulting output files occupy, this level of refinement would be too great computationally. Therefore calculations with steps of 5% were done, again with the expectation that any change in band gap is continuous and not sporadic, and subsequent interesting results would be examined in greater detail.

CHAPTER III

RESULTS

In this chapter, the results of the effect of strain on the band gap of graphene are presented. A convergence study is first conducted to obtain the necessary variables to use in ABINIT. The band gaps for uniaxial, biaxial, shear, and angular strain are calculated, as well as for the total strain space.

3.1 Convergence

The pseudopotential used for calculations was from Troullier and Martins [24], created with the JL Martins psp generator. This pseudopotential uses the local density approximation (LDA) [25] of the exchange correlation energy functional. LDA approximations are known to underestimate band gaps, and results are expected to be lower than the experimental value [26, 27].

In order to ensure that the computational model represented in ABINIT is accurate, certain variables need to be converged for a given pseudopotential. We use the periodic boundary conditions described in Section 2.4 such that we can specify a single unit cell and have it replicated periodically. `acell` is the variable that multiplies the lattice vectors of unit length by a scalar to achieve the correct unit cell size. The values are given as an array where the value in `acell` multiplies the corresponding lattice vector value.

Table 1: Convergence data for acell and ecut in graphene

	Ecut	Acell	Energy Per Atom (eV)	Binding Energy Per Atom (eV)
Ecut Convergence	20	2.65998 2.65998 30	-155.60257	-10.15074
	22	2.65998 2.65998 30	-155.60572	-10.15390
	24	2.65998 2.65998 30	-155.60686	-10.15503
	26	2.65998 2.65998 30	-155.60601	-10.15418
	28	2.65998 2.65998 30	-155.60328	-10.15145
	30	2.65998 2.65998 30	-155.60572	-10.15390
	32	2.65998 2.65998 30	-155.60686	-10.15503
	34	2.65998 2.65998 30	-155.60601	-10.15418
Acell Convergence	34	2.64 2.64 30	-155.60257	-10.15074
	34	2.65 2.65 30	-155.60572	-10.15390
	34	2.66 2.66 30	-155.60686	-10.15503
	34	2.67 2.67 30	-155.60601	-10.15418
	34	2.68 2.68 30	-155.60328	-10.15145

The variable ecut affects the accuracy of calculations as the planewave energy cutoff. The total energy will decrease as ecut increases and approach the true minimum, and a value needs to be found where the difference between the last two values is acceptably small and the minimum is therefore closely approximated. The energy of a single Carbon atom was found to be -145.45182 eV and is used in Table 1 by being subtracted from the total energy per atom to obtain the binding energy per atom. The binding energy per atom has converged at an energy cutoff of 34 Ha, with a 0.0016 eV difference between that and the penultimate value.

From Table 1, The relationship of the value for acell vs. total energy was approximated to the third order by $f(x) = -23.65x^3 + 208.39x^2 - 606.62x + 273.07$. The goal of convergence

is to find the minimum energy, which is where the system is in equilibrium, and the distances between atoms are the lattice constants. The minimum energy was found by taking $\frac{df(x)}{dx} = 0$. The resulting critical point was 2.65998 Bohr, which gives the acell value for the zigzag and armchair directions. 2.65998 Bohr is 1.4076 Å, which is in close agreement with the experimental value of 1.42 Å. The stresses were also checked for this value, as they should be negligibly small when acell is converged. The resulting stresses are (in GPa):

$$\sigma = \begin{pmatrix} -4.83784E - 03 & 0 & 0 \\ 0 & -4.83784E - 03 & 0 \\ 0 & 0 & 7.09922E - 02 \end{pmatrix}.$$

An arbitrarily large acell value of 30 Bohr was chosen for the out-of-plane direction, in order to ensure that no interaction occurs between sheets. The values of acell are thus (2.65998, 2.65998, 30). In this case, $\bar{a}_1 = a_0(\frac{\sqrt{3}}{2}, \frac{3}{2}, 0)$ and $\bar{a}_2 = a_0(-\frac{\sqrt{3}}{2}, \frac{3}{2}, 0)$ are the lattice vectors and acell gives the equilibrium lattice dimensions. The unit cell is therefore:

$$\begin{aligned} \bar{a}_1 &= 2.65998(\frac{\sqrt{3}}{2}, \frac{3}{2}, 0) \\ \bar{a}_2 &= 2.65998(-\frac{\sqrt{3}}{2}, \frac{3}{2}, 0) \\ \bar{a}_3 &= 30(0, 0, 1). \end{aligned}$$

3.2 Uniaxial Strain

Normal strain in the zigzag direction is described by the following strain tensor:

$$\mathbf{E} = \begin{pmatrix} \varepsilon & 0 & 0 \\ 0 & 0 & 0 \\ 0 & 0 & 0 \end{pmatrix}.$$

As seen in Figure 4, gap does not open under uniaxial strain in the zigzag direction.

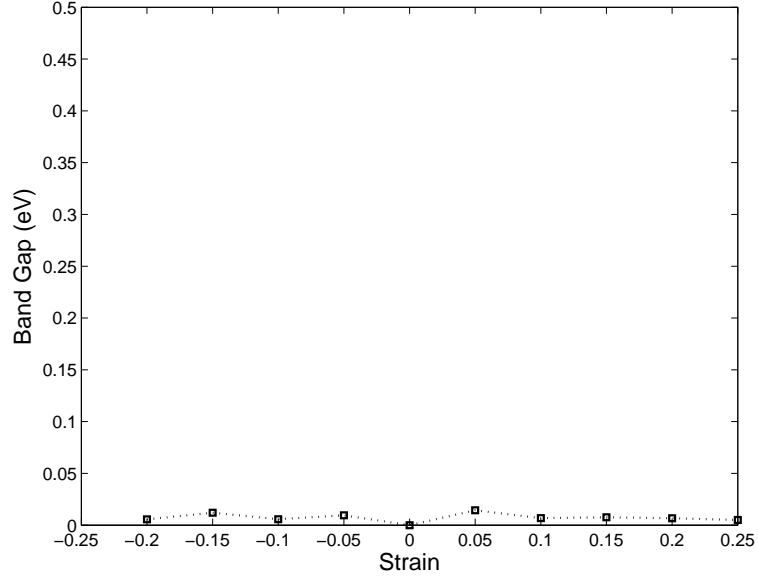


Figure 4: Strain vs. band gap for uniaxial strain in zigzag direction

Normal strain in the armchair direction is described by the following strain tensor:

$$\mathbf{E} = \begin{pmatrix} 0 & 0 & 0 \\ 0 & \varepsilon & 0 \\ 0 & 0 & 0 \end{pmatrix}.$$

As seen in Figure 5, gap of 0.2623 eV opens under 25% uniaxial strain in the armchair direction. This is impractical however, considering graphene's mechanical limits [21, 20].

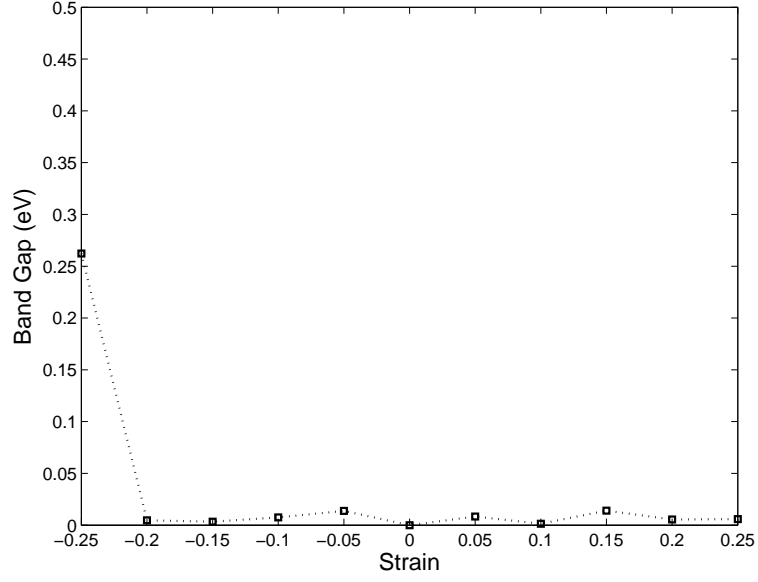


Figure 5: Strain vs. band gap for uniaxial strain in armchair direction

3.3 Biaxial Strain

Biaxial normal strain in both the zigzag and armchair directions is described by the following strain tensor:

$$\mathbf{E} = \begin{pmatrix} \varepsilon & 0 & 0 \\ 0 & \varepsilon & 0 \\ 0 & 0 & 0 \end{pmatrix}.$$

As seen in Figure 6, gap does not open under biaxial strain. The results for uniaxial and biaxial strain are in agreement with recent literature, as a gap begins to open well past 20% strain [12, 9] in the armchair direction.

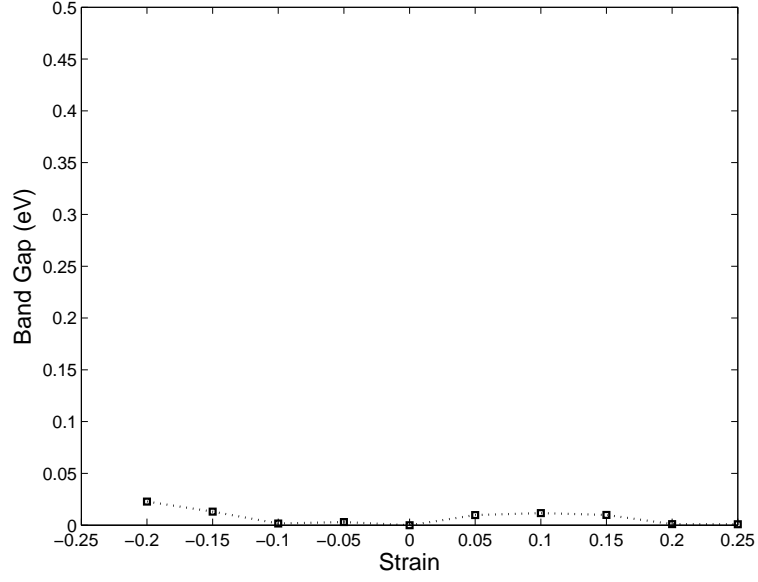


Figure 6: Strain vs. band gap for biaxial strain

3.4 Shear Strain

Shear strain is described by the following strain tensor:

$$\mathbf{E} = \begin{pmatrix} 0 & \varepsilon & 0 \\ \varepsilon & 0 & 0 \\ 0 & 0 & 0 \end{pmatrix}.$$

As seen in Figure 7, gap of 0.4014 eV opens when $\varepsilon=0.2$ and -0.2 . These are uniform strains below the mechanical limit that open a band gap, contrary to claims in literature [9], but are not extremely large, nor can they be modulated significantly.

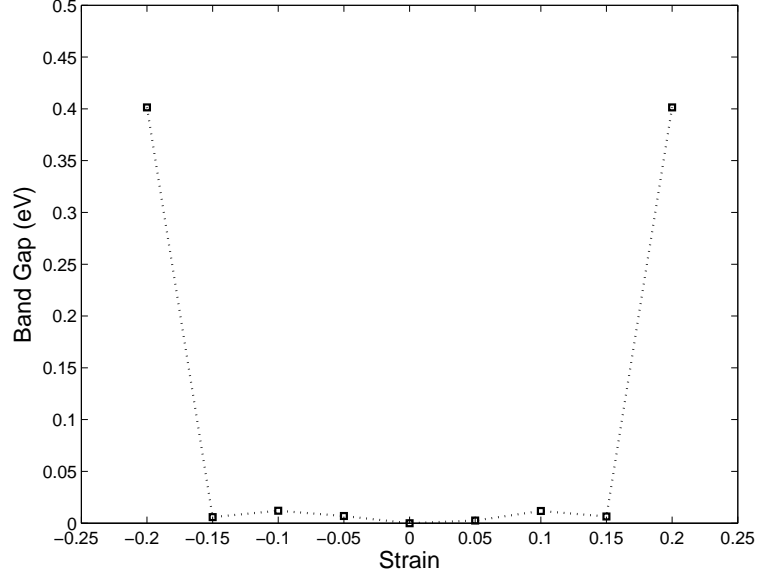


Figure 7: Strain vs. band gap for shear strain

3.5 *Angular Uniaxial Strain*

The strain tensor for angular axial strain was obtained by rotating the strain tensor for the uniaxial case in the zigzag direction. Due to the symmetry of the hexagonal lattice, pulling in the direction with angle α in the region bounded by the atom and midway between atoms is equivalent to pulling in any other region in the direction α bounded by another atom and midway to another atom. This means that i) the periodicity for pulling in the direction of an angle θ is 30° , and ii) it is equivalent to pick either the zigzag or armchair direction when defining $\theta = 0$. The rotation matrix is given by:

$$\mathbf{R} = \begin{pmatrix} \cos\theta & -\sin\theta & 0 \\ \sin\theta & \cos\theta & 0 \\ 0 & 0 & 1 \end{pmatrix}$$

which rotates the strain tensor corresponding to normal strain in the zigzag direction:

$$\mathbf{E} = \begin{pmatrix} \varepsilon & 0 & 0 \\ 0 & 0 & 0 \\ 0 & 0 & 0 \end{pmatrix}.$$

This gives a rotation θ about the out-of-plane axis in the zigzag-armchair plane. The rotated strain tensor is found by:

$$\mathbf{E}' = \mathbf{R}\mathbf{E}\mathbf{R}^T$$

As seen in Figures 8, 9, and 10, a gap does not open under angular uniaxial tension.

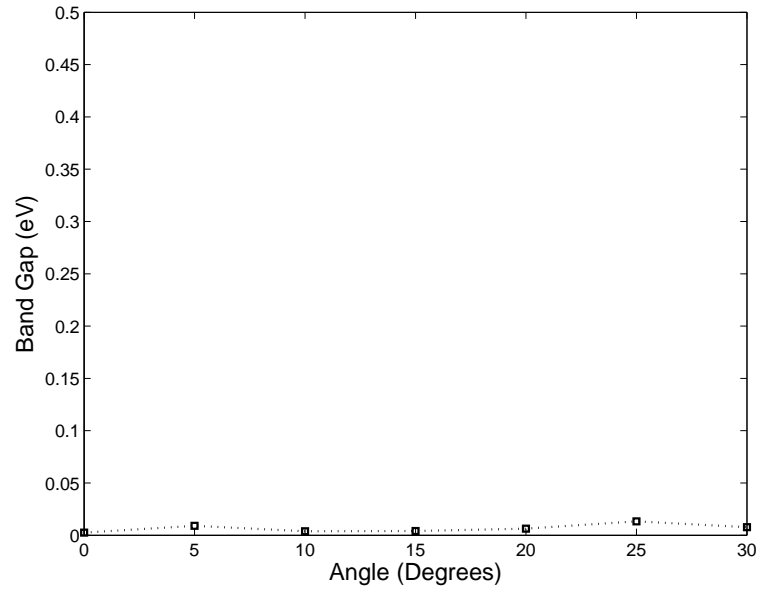


Figure 8: Angle vs. band gap for uniaxial strain when $\varepsilon = 0.1$

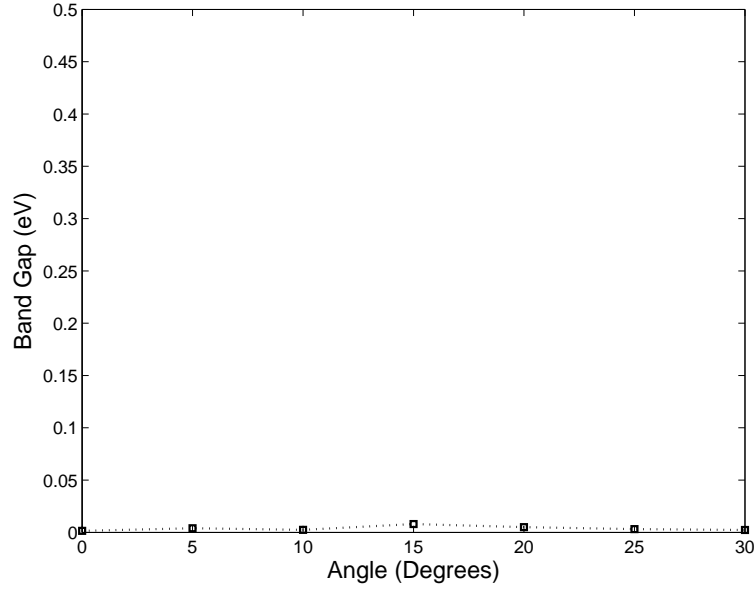


Figure 9: Angle vs. band gap for uniaxial strain when $\varepsilon = 0.15$

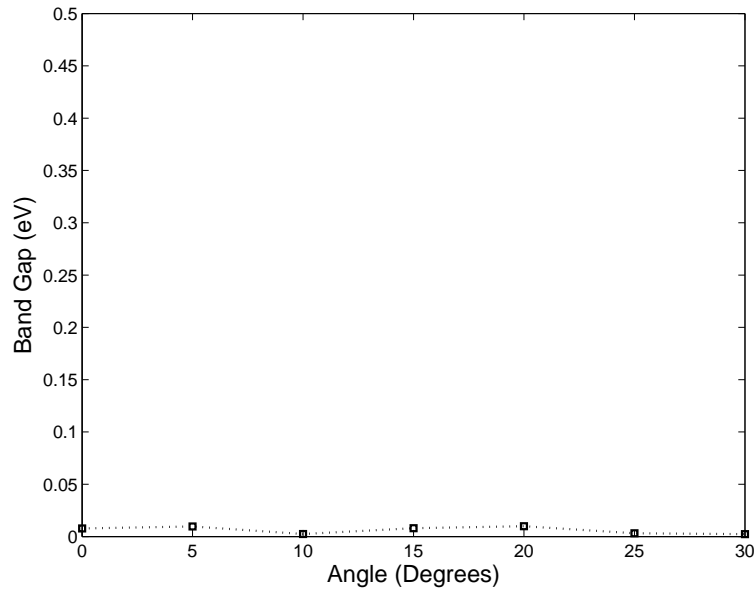


Figure 10: Angle vs. band gap for uniaxial strain when $\varepsilon = 0.2$

3.6 *Traversal of In-Plane Strain Space*

After the calculations for all the permutations mentioned in Section 2.6 were complete, the resulting data were filtered to obtain strains that were of great interest. 13 input files were identified, seen in Table 2, as having band gaps greater than 0.2 eV, while each of the

principal strains associated with those deformation gradients were still under 20%. These points indicated that asymmetrical biaxial strain would be the preferred method of opening a band gap.

Table 2: States of strain with high band gaps

ε_{11}	ε_{12}	ε_{21}	ε_{22}	Band Gap (eV)
-0.15	-0.10	-0.10	0.10	0.4109
-0.15	-0.10	-0.10	0.15	0.6057
-0.15	0.10	0.10	0.10	0.4108
-0.15	0.10	0.10	0.15	0.6049
-0.10	-0.15	-0.15	0.05	0.5442
-0.10	0.15	0.15	0.05	0.5442
-0.05	-0.15	-0.15	0.05	0.4340
-0.05	-0.15	-0.15	0.10	0.2978
-0.05	0.15	0.15	0.05	0.4342
-0.05	0.15	0.15	0.10	0.2978
0.10	0	0	-0.20	0.9229
0.15	0	0	-0.20	0.3510
0.15	0	0	0.15	0.2485

3.7 *Asymmetrical Biaxial Strain*

Following the results of Table 2, calculations were refined to include all permutations of biaxial strain in steps of 1%, while having a minimum of -0.2 and a maximum of 0.2 in both armchair and zigzag directions. Asymmetrical biaxial strain in the armchair and zigzag directions is described by the following strain tensor:

$$\mathbf{E} = \begin{pmatrix} \varepsilon_{zz} & 0 & 0 \\ 0 & \varepsilon_{ac} & 0 \\ 0 & 0 & 0 \end{pmatrix},$$

where $\varepsilon_{ac} \neq \varepsilon_{zz}$. A band gap of 1.0087 eV has been observed in asymmetrical biaxial strain with $\varepsilon_{11} = 0.11$ and $\varepsilon_{22} = 0.2$, seen in Figures 11 and 12. Any gap is routinely opened at the M point, the high symmetry point corresponding to $(\frac{1}{2}, \frac{1}{2}, 0)$ in the Brillouin zone.

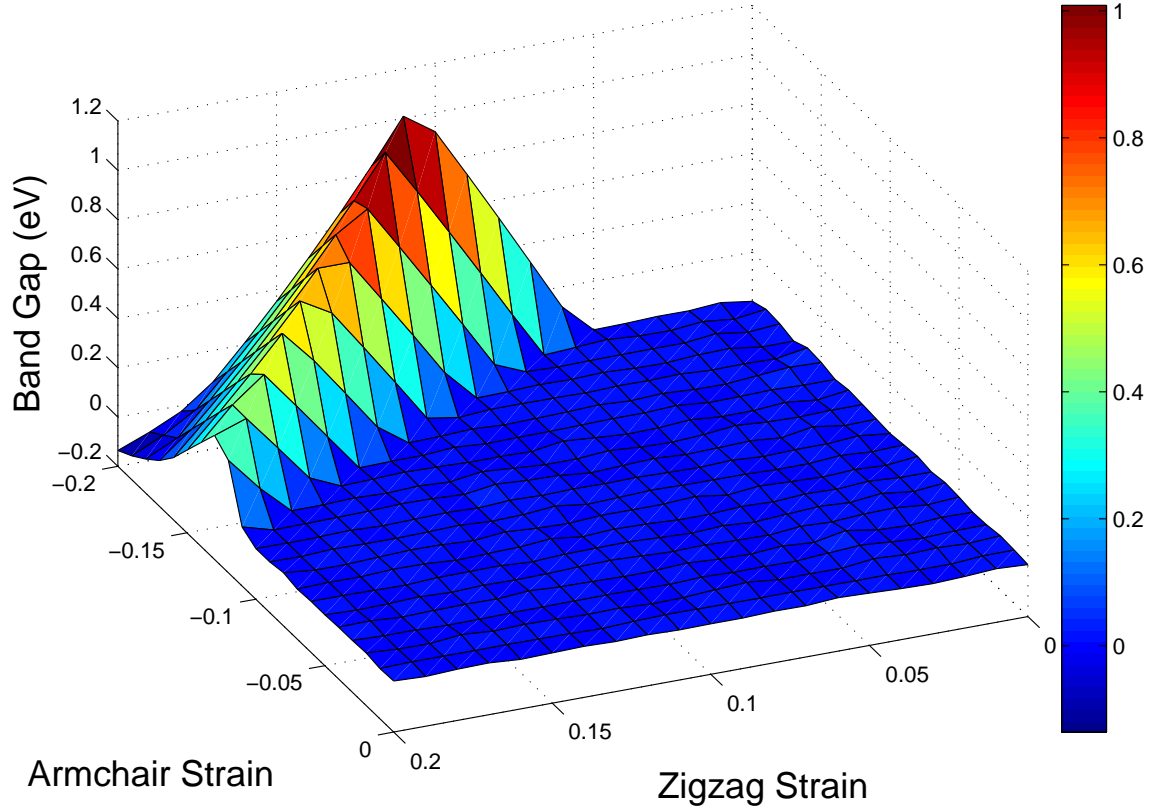


Figure 11: Graphical representation of band gap opening as a function of ε_{ac} and ε_{zz}

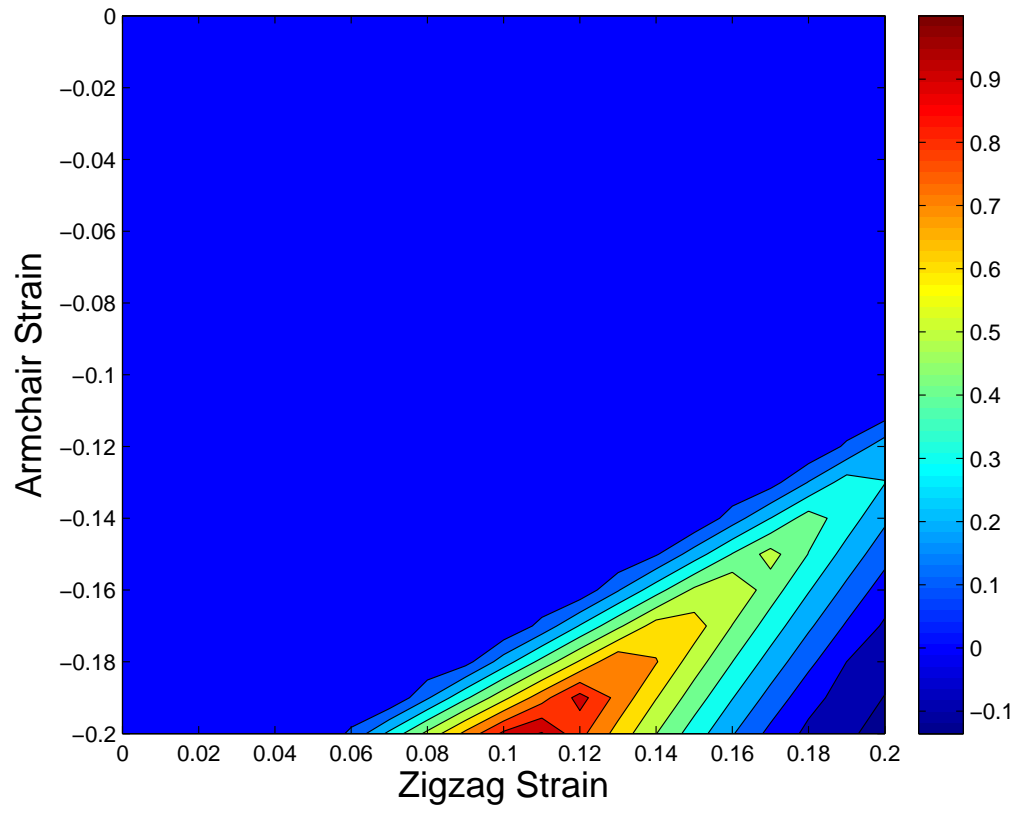


Figure 12: Graphical representation of band gap opening as a function of ε_{ac} and ε_{zz}

CHAPTER IV

CONCLUSION

Table 2 indicates that it is possible to open and modulate a gap with a combination of shear and biaxial strains. However, the highest band gaps are not found with shear present. Furthermore, to obtain the highest gaps it is necessary that the strain in the armchair direction be compressive and the strain in the zigzag direction tensile. We conclude that, using Figures 11 and 12, it is possible to strain engineer graphene to exhibit a band gap of up to ≈ 1 eV by using ε_{11} between ≈ 0.06 and ≈ 0.2 and ε_{22} between ≈ -0.12 and ≈ -0.2 .

APPENDIX A

SAMPLE ABINIT INPUT FILE

Abinit input file for 10% uniaxial strain:

Dataset 1: Self consistent calculation

rprim1

0.94868329805051 1.5000000000000000 0.0000000000000000

-0.94868329805051 1.5000000000000000 0.0000000000000000

0.000000 0.000000 1.000000

kptopt1 1

nshiftk1 1

shiftk1 0 0 0

ngkpt1 20 20 1

prtden1 1

toldfe1 1.0d-9

Dataset 2: Band structure

rprim2

0.94868329805051 1.5000000000000000 0.0000000000000000

-0.94868329805051 1.5000000000000000 0.0000000000000000

0.000000 0.000000 1.000000

iscf2 -2

getden2 -1

kptopt2 0

shiftk2 0 0 0

prtden2 0

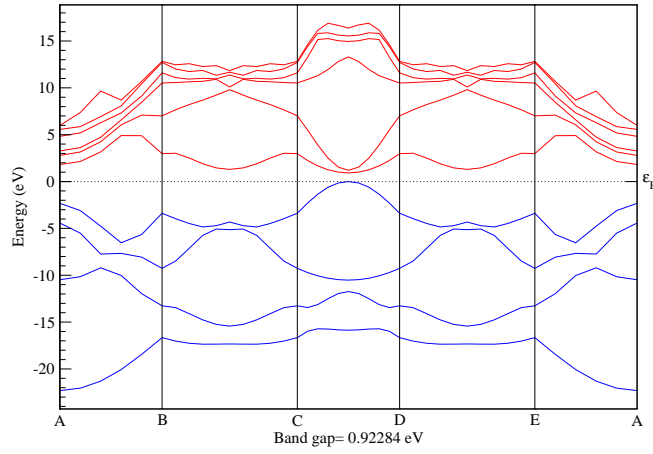
tolwfr2 1.0d-12

```
nkpt2 9999
kpt2
0.35685317512053 0.63923214294701 0.0000000000000000
0.34156999035061 0.61782212024063 0.0000000000000000
# The remaining k-points have been suppressed due to space
# Common parameters for all datasets
ndtset 2
enunit 1
prtwf 0
nband 8
acell 2.65998 2.65998 30
ntypat 1
znucl 6
natom 2
typat 1 1
xred
1/3 1/3 0
2/3 2/3 0
ecut 34
nstep 40
diemac 12
```

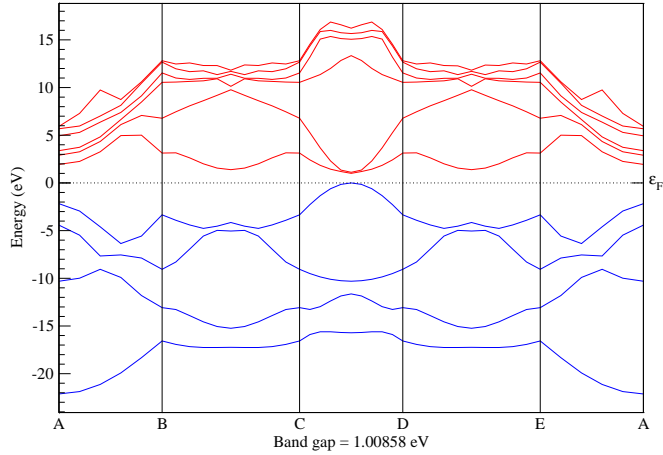
APPENDIX B

BAND STRUCTURE PLOTS

The following graphs depict the band structure of strained graphene for the four highest band gap values obtained in Figures 11 and 12.

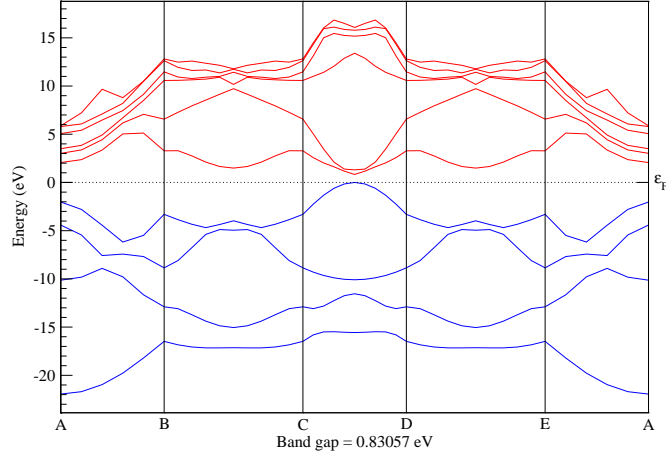


(a) $\varepsilon_{11} = 0.1, \varepsilon_{22} = -0.2$

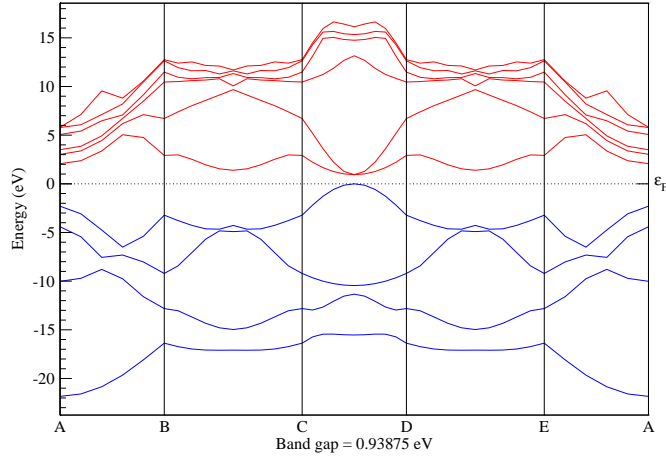


(b) $\varepsilon_{11} = 0.11, \varepsilon_{22} = -0.2$

Figure 13: Band structure plots of a sample of strain states with high band gaps. $A = (0, 0, 0)$ $B = (\frac{1}{3}, -\frac{1}{3}, 0)$ $C = (\frac{2}{3}, \frac{1}{3}, 0)$ $D = (\frac{1}{3}, \frac{2}{3}, 0)$ $E = (-\frac{1}{3}, \frac{1}{3}, 0)$. It can be seen that the high symmetry points where the gap is 0 in unstrained graphene (A, B, C, D, and E) have opened considerably, but the gap at the M point ($\frac{1}{2}, \frac{1}{2}, 0$) between C and D has closed from ≈ 4.1 eV in the unstrained system to the values shown above.



(a) $\varepsilon_{11} = 0.12, \varepsilon_{22} = -0.2$



(b) $\varepsilon_{11} = 0.11, \varepsilon_{22} = -0.19$

Figure 14: Band structure plots of a sample of strain states with high band gaps. $A = (0, 0, 0)$ $B = (\frac{1}{3}, -\frac{1}{3}, 0)$ $C = (\frac{2}{3}, \frac{1}{3}, 0)$ $D = (\frac{1}{3}, \frac{2}{3}, 0)$ $E = (-\frac{1}{3}, \frac{1}{3}, 0)$. It can be seen that the high symmetry points where the gap is 0 in unstrained graphene (A, B, C, D, and E) have opened considerably, but the gap at the M point $(\frac{1}{2}, \frac{1}{2}, 0)$ between C and D has closed from ≈ 4.1 eV in the unstrained system to the values shown above.

Bibliography

- [1] M. I. Katsnelson and M. I. Katsnelson, *Graphene: carbon in two dimensions*. Cambridge University Press, 2012.
- [2] J. H. Warner, F. Schaffel, M. Rummeli, and A. Bachmatiuk, *Graphene: fundamentals and emergent applications*. Newnes, 2012.
- [3] S. K. Pati, T. Enoki, and C. N. R. Rao, *Graphene and its fascinating attributes*. World Scientific, 2011.
- [4] P. Avouris and C. Dimitrakopoulos, “Graphene: synthesis and applications,” *Materials today*, vol. 15, no. 3, pp. 86–97, 2012.
- [5] V. Singh, D. Joung, L. Zhai, S. Das, S. I. Khondaker, and S. Seal, “Graphene based materials: Past, present and future,” *Progress in Materials Science*, vol. 56, no. 8, pp. 1178 – 1271, 2011.
- [6] S. Zhou, G.-H. Gweon, A. Fedorov, P. First, W. De Heer, D.-H. Lee, F. Guinea, A. C. Neto, and A. Lanzara, “Substrate-induced bandgap opening in epitaxial graphene,” *Nature materials*, vol. 6, no. 10, pp. 770–775, 2007.
- [7] Y. Zhang, T.-T. Tang, C. Girit, Z. Hao, M. C. Martin, A. Zettl, M. F. Crommie, Y. R. Shen, and F. Wang, “Direct observation of a widely tunable bandgap in bilayer graphene,” *Nature*, vol. 459, no. 7248, pp. 820–823, 2009.
- [8] E. V. Castro, K. Novoselov, S. Morozov, N. Peres, J. L. Dos Santos, J. Nilsson, F. Guinea, A. Geim, and A. C. Neto, “Biased bilayer graphene: semiconductor with a gap tunable by the electric field effect,” *Physical Review Letters*, vol. 99, no. 21, p. 216802, 2007.
- [9] I. Naumov and A. Bratkovsky, “Gap opening in graphene by simple periodic inhomogeneous strain,” *Physical Review B*, vol. 84, no. 24, p. 245444, 2011.

- [10] Z. H. Ni, T. Yu, Y. H. Lu, Y. Y. Wang, Y. P. Feng, and Z. X. Shen, “Uniaxial strain on graphene: Raman spectroscopy study and band-gap opening,” *ACS nano*, vol. 2, no. 11, pp. 2301–2305, 2008.
- [11] G. Gui, J. Li, and J. Zhong, “Band structure engineering of graphene by strain: First-principles calculations,” *Phys. Rev. B*, vol. 78, p. 075435, Aug 2008.
- [12] S.-M. Choi, S.-H. Jhi, and Y.-W. Son, “Effects of strain on electronic properties of graphene,” *Phys. Rev. B*, vol. 81, p. 081407, Feb 2010.
- [13] V. M. Pereira, A. C. Neto, and N. Peres, “Tight-binding approach to uniaxial strain in graphene,” *Physical Review B*, vol. 80, no. 4, p. 045401, 2009.
- [14] G. Cocco, E. Cadelano, and L. Colombo, “Gap opening in graphene by shear strain,” *Phys. Rev. B*, vol. 81, p. 241412, Jun 2010.
- [15] F. Schwierz, “Graphene transistors,” *Nature nanotechnology*, vol. 5, no. 7, pp. 487–496, 2010.
- [16] W. Kohn and L. J. Sham, “Self-consistent equations including exchange and correlation effects,” *Phys. Rev.*, vol. 140, pp. A1133–A1138, Nov 1965.
- [17] Z. H. Ni, T. Yu, Y. H. Lu, Y. Y. Wang, Y. P. Feng, and Z. X. Shen, “Uniaxial strain on graphene: Raman spectroscopy study and band-gap opening,” 2009.
- [18] X. Gonze, B. Amadon, P.-M. Anglade, J.-M. Beuken, F. Bottin, P. Boulanger, F. Bruneval, D. Caliste, R. Caracas, M. Cote, *et al.*, “Abinit: First-principles approach to material and nanosystem properties,” *Computer Physics Communications*, vol. 180, no. 12, pp. 2582–2615, 2009.
- [19] X. Gonze, “A brief introduction to the abinit software package,” *Zeitschrift für Kristallographie*, vol. 220, no. 5/6/2005, pp. 558–562, 2005.
- [20] C. Lee, X. Wei, J. W. Kysar, and J. Hone, “Measurement of the elastic properties and intrinsic strength of monolayer graphene,” *science*, vol. 321, no. 5887, pp. 385–388, 2008.

- [21] F. Liu, P. Ming, and J. Li, “Ab initio calculation of ideal strength and phonon instability of graphene under tension,” *Physical Review B*, vol. 76, no. 6, p. 064120, 2007.
- [22] J. N. Reddy, *An introduction to continuum mechanics*. Cambridge university press, 2013.
- [23] N. W. Ashcroft, N. D. Mermin, and S. Rodriguez, *Solid State Physics*, vol. 46. American Association of Physics Teachers, 1978.
- [24] N. Troullier and J. L. Martins, “Efficient pseudopotentials for plane-wave calculations,” *Phys. Rev. B*, vol. 43, pp. 1993–2006, Jan 1991.
- [25] E. K. U. Gross and W. Kohn, “Local density-functional theory of frequency-dependent linear response,” *Phys. Rev. Lett.*, vol. 55, pp. 2850–2852, Dec 1985.
- [26] P. Scharoch and M. Winiarski, “An efficient method of dft/lda band-gap correction,” *Computer Physics Communications*, vol. 184, no. 12, pp. 2680–2683, 2013.
- [27] H. Xiao, J. Tahir-Kheli, and W. A. Goddard III, “Accurate band gaps for semiconductors from density functional theory,” *The Journal of Physical Chemistry Letters*, vol. 2, no. 3, pp. 212–217, 2011.